Small-Angle X-ray Scattering (SAXS) Studies of Sulfonated Polystyrene Ionomers. 2. Correlation Function Analysis

Dan Q. Wu† and Benjamin Chu*

Chemistry Department, State University of New York at Stony Brook, Long Island, New York 11794-3400

Robert D. Lundberg

Corporate Research Science Laboratory, Exxon Research and Engineering Company, Clinton Township, Route 22 East, Annandale, New Jersey 08801

William J. MacKnight

Department of Polymer Science and Engineering, University of Massachusetts, Amherst, Massachusetts 01003

Received June 1, 1992; Revised Manuscript Received October 13, 1992

ABSTRACT: Small-angle X-ray scattering (SAXS) profiles of ionomers often show a typical scattering peak located at $q \sim 1$–3 nm^{-1} due to ionic aggregation and a zero-order scattering upturn. Anomalous SAXS (ASAXS) has confirmed that such an upturn is due to ions. The structure of ionic aggregates and the spatial arrangement of ions can best be elucidated by the correlation function analysis of precise SAXS profiles which have a wide scattering angular range and a high spatial resolution. Electron density–density correlation functions of sulfonated polystyrene (SPS) sodium and zinc salts (4.5 mol % of sulfur, 100% neutralization, and $M_w/M_n = 1.2$) have been computed from the SAXS profiles. The results showed that the short-range structure could be described by the liquidlike model, while the long-range structure could be fitted approximately (and empirically) by invoking a Debye–Bueche type random inhomogeneity model.

I. Introduction

In the previous paper (referred to as paper 1, in which all pertinent references on anomalous small-angle X-ray scattering have been cited), we have established how SAXS profiles of Zn in sulfonated polystyrenes (SPS) can be determined either by anomalous small-angle X-ray scattering (ASAXS) using X-ray energies near and away from the absorption edge of a specific element such as Zn or by small-angle X-ray scattering (SAXS) using the SAXS profile from polystyrene (PS) as the background. In the present paper, we want to use the SAXS profiles of SPS-Na and -Zn for comparison with some existing ionomer models based on the correlation function analysis.

For the lack of structure in the SAXS profiles of ionomers, it has been very difficult to distinguish the different proposed models which depict the ionomer structures because all of the models can produce an ionic peak. However, in a more detailed analysis of the models in r-space, instead of q-space, we have noted distinct features among the models. The differences, though small, can provide the means to a closer comparison between experimental data and the proposed ionomer models (in r-space) provided that high-quality SAXS profiles could be measured over a broad enough q-range. Therefore, although we present only a limited number of SAXS profiles for the correlation function profile analysis (in r-space), our data represent, at this time, the most precise SAXS measurements over a q-range which is sufficiently broad for a Fourier transform of the scattering data into r-space without any model-dependent assumptions. However, we do have to arbitrarily separate the scattering data into two incoherent contributions because of the strong small-angle upturn.

This paper is divided into the following sections: II. Intensity-Structure Relations, III. Numerical Computation of the Correlation Function, IV. Ionomer Morphological Models, and V. Results and Discussion.

II. Intensity–Structure Relations

For a real molecular system, the scattered intensity, $I(q)$, is expressed by a complex conjugate of the scattering amplitude, $F(q)$, i.e.

$$I(q) = F(q)\,F^*(q) = \int\int \rho(\mathbf{r}_1)\,\rho(\mathbf{r}_2)\,\exp(i\mathbf{q}\cdot(\mathbf{r}_2-\mathbf{r}_1))\,d^3\mathbf{r}_1\,d^3\mathbf{r}_2 \quad (1)$$

where $\mathbf{q}$ is the scattering vector and $|q| = (4\pi/\lambda)\sin(\theta/2)$, with λ and θ being respectively the X-ray wavelength and the scattering angle, and $\rho(\mathbf{r})$ is the electron density function of the system. Equation 1 can be written as

$$I(\mathrm{q}) = \int \rho^2(r)\,\exp(i\mathbf{q}\cdot\mathbf{r})\,d^3r \quad (2)$$

where $\rho^2(r) = \int\rho(\mathbf{r}_1)\,\rho(\mathbf{r}_2)\,d^3r_1$, with $r = |\mathbf{r}_1 - \mathbf{r}_2|$. If the system is statistically isotropic, the three-dimensional integration in eq 2 can be simplified by averaging all possible orientations of $\mathbf{q}$ with respect to $\mathbf{r}$. Thus

$$I(q) = 4\pi\int_0^\infty r^2\rho^2(r)\,\frac{\sin qr}{qr}\,dr \quad (3)$$

Debye and Bueche[1] proposed the use of a local electron density fluctuation, $\eta(r) = \rho(r) - \langle\rho(r)\rangle$, to replace the electron density $\rho(r)$ in eqs 1 and 2. The correlation function, $\gamma(r)$, is defined as $\gamma(r) = \langle\eta(\mathbf{r}_1)\,\eta(\mathbf{r}_2)\rangle$. Then, eq 3 has the form

$$I(q) = 4\pi\int_0^\infty r^2\gamma(r)\,\frac{\sin qr}{qr}\,dr \quad (4)$$

where $\gamma(r)$ can be determined by an inverse Fourier transform:

$$\gamma(r) = (1/2\pi^2)\int_0^\infty q^2 I(q)\,\frac{\sin qr}{qr}\,dq \quad (5)$$

* Author to whom correspondence should be addressed.
† Present address: Polymer Products Department, Du Pont Experimental Station, Wilmington, DE 19880-0269.

0024-9297/93/2226-1000$04.00/0

When $q = 0$, eq 5 has a simple form:

$$\gamma(0) = (1/2\pi^2)\int_0^\infty q^2 I(q)\,dq = \langle\eta^2\rangle \quad (6)$$

$\gamma(0)$ is the mean-square electron density fluctuations and leads to a very important parameter of the system, Q, known as the invariant.

$$Q = \int_0^\infty q^2 I(q)\,dq \quad (7)$$

Q is constant if the mean-square electron density is unchanged, irrespective of the change of structural features like shape that may accompany a significant change in $I(q)$.

For a system with random inhomogeneities, the electron density fluctuation correlation function has the form[1]

$$\gamma_{D\text{-}B}(r) = \langle\eta^2\rangle \exp(-r/a) \quad (8)$$

with a being the correlation length characterizing the system inhomogeneity. The subscript D–B denotes the Debye–Bueche model. The scattered intensity corresponding to eq 8 can be obtained easily by using eq 4:

$$I_{D\text{-}B}(q) = \frac{8\pi\langle\eta^2\rangle a^3}{(1 + a^2q^2)^2} \quad (9)$$

Equations 8 and 9 have been applied to a variety of random systems[1-4] as well as to ionomers.[5,6] The correlation length a can be determined from a plot of $I^{1/2}$ vs q^2 at small scattering angles.

If a SAXS profile covers a broad q range, i.e., from $q_{min} \sim 0$ to a q_{max} where $I(q_{max}) \sim 0$, the correlation function defined by eq 5 can be determined from $I(q)$. The correlation function could provide the most direct information about the structure that brings about the scattering profile.

Application of eqs 4 and 5 requires knowledge of the absolute scattered intensity. For relative scattered intensity, an alternative definition of the correlation function is needed:

$$\gamma_N(r) = \langle\eta(\mathbf{r}_1)\,\eta(\mathbf{r}_2)\rangle/\langle\eta^2\rangle, \quad \text{with } r = |\mathbf{r}_1 - \mathbf{r}_2| \quad (10)$$

where for simplicity we shall drop the subscript N. The relation of $\gamma(r)$ to the scattered intensity is given by

$$\gamma(r) = \int_0^\infty q^2 I(q)\frac{\sin qr}{qr}\,dq/Q \quad (11)$$

where the invariant Q has been defined by eq 7. The inverse Fourier transform of eq 11 has a slightly different form from eq 4, i.e.

$$I(q) = (2/\pi)Q\int_0^\infty r^2\gamma(r)\frac{\sin qr}{qr}\,dr \quad (12)$$

Since SAXS can only cover a finite q range, e.g., from q_{min} to q_{max}, the correlation function $\gamma'(r)$ is defined by

$$\gamma'(r) = \int_{q_{min}}^{q_{max}} q^2 I(q)\frac{\sin qr}{qr}\,dq/Q' \quad (13)$$

with

$$Q' = \int_{q_{min}}^{q_{max}} q^2 I(q)\,dq \quad (14)$$

It is clear that $\gamma(r) \cong \gamma'(r)$, if $q_{min} \sim 0$ and $I(q_{max}) \sim 0$. Usually, q_{min} can be extrapolated to zero by using either the Guinier approximation[7] or the Debye–Bueche random inhomogeneity approach (eq 9).

III. Numerical Computation of the Correlation Function

Equation 13 can be solved numerically by using a fast Fourier transform (FFT) algorithm[8] or a numerical integration method (NIM) which is slower but has a higher r resolution.[9] While FFT uses

$$\gamma'(r_j) = (1/Q'r_j)\,\delta_q\sum_{k=1}^{N} q_k I(q_k)\sin(2\pi jk/N), \quad j = 1, 2, ..., N/2 \quad (15)$$

where

$$q_k = k\,\delta q, \quad r_j = j\,\delta r, \quad r_{min} = \delta r = 2\pi/q_{max}, \quad r_{max} = 2\pi/\delta q$$

and $\sin(2\pi jk/N) = \sin(jk\,\delta r\,\delta q)$. NIM improves the resolution in r by a factor of 2

$$\gamma'(r_j) = (1Q'r_j)\,\delta q\sum_{k=1}^{N} q_k I(q_k)\sin(q_k r_j), \quad j = 1, 2, ..., N \quad (16)$$

with

$$q_k = k\,\delta q, \quad r_j = j\,\delta r, \quad r_{min} = \delta r = \pi/q_{max}, \quad r_{max} = \pi/\delta q$$

The resolution improvement by NIM is quite important. For example, if $q_{max} = 10.0$ nm^{-1}, FFT gives $r_{min} = 2\pi/q_{max} = 0.628$ nm, while NIM offers $r_{min} = 0.314$ nm. The computation speed difference is usually no more than 1–2 min on an IBM PC/AT.

Equations 15 and 16 would generate high-frequency oscillations in γ because of the roughness of experimental data or a high q termination, i.e., $I(q_{max}) \neq 0$. The former can be avoided by smoothing the data while the latter can be improved by appending a Gaussian damping function like $\exp(-\alpha q^2)$ to the tail of the curve so as to extend the data to a q_∞ ($>q_{max}$). α can be chosen, for example, to have $\exp(-\alpha q_\infty^2) = I(q_{max}) \times 10^{-n}$, with $n = 4$ or 5.

The choice of damping function should not make any difference in the final "smoothed" correlation function. It should be emphasized, however, that the closer the value of $I(q_{max})$ is to zero, the less ambiguous the result becomes.

The methods for smoothing SAXS profiles can be selected from a low-pass filter,[10] a cubic-spline smoother,[11] or a piecewise rotationally resistant smoother.[12] The quality of the smoothing is judged by whether the smoothed curve goes through the fluctuated data points. The structural properties determined should not depend on the choice of the smoothing method.

An alternative method for solving eq 13 is to use a maximum entropy method (MEM).[13-15] The algorithm which does not require data smoothing and takes into account the statistics of each data point might be the best-known, least-biased method for solving inverse problems in general. We have not yet implemented the MEM to the present problem.

IV. Ionomer Morphological Models

Most models proposed to describe the structures of ionic aggregates in ionomers were based on the interpretation of a single broad SAXS diffraction peak which is usually located at a scattering angle corresponding to a q value ranging from 0.5 to 4 nm^{-1}. The peak has been observed for almost all ionomer systems. In fact, the ionic peak has become an indicator of the presence of ionic aggregation. MacKnight and Earnest[16] have reviewed several morphological models proposed prior to 1980. Recently, Mauritz[17] summarized a few newer models which emphasized the applications in perfluoro ionomers.

A few selected models will be discussed and computer simulated. The first effort to describe physically the formation of ionic aggregates in ionomers was given by Eisenberg,[18] who has since revised his ideas to form a new multiplet-cluster model for the morphology of random ionomers.[19] The fundamental concepts of ionic aggregation, such as ion pairs, ion multiplets, and ion clusters, are commonly used to interpret the experimental results.

Ion pairs were the primary units. A cation and an anion were assumed to be separated by a distance corresponding to their ionic radii. A multiplet was defined as an aggregate of ion pairs without mixing with hydrocarbon chains. The maximum number of the ion pairs in a multiplet could be calculated based on the balance between the energetically favored aggregation of ion pairs and the steric hindrance consequently caused by the interaction between hydrocarbon polymer backbones. A cluster was then formed by a loose association among several multiplets resulting from a competition between the loss of conformational entropy of the polymer when the clustering occurs and electrostatic interactions.

IV.1. Core-Shell Model.[20] On the basis of a radial distribution function analysis of X-ray scattering profiles of carboxylate ionomers[21] at both small and wide scattering angles and other experimental data, MacKnight et al.[20] identified the broad diffraction peak as the result of ionic aggregation and attributed the ionic peak to the interference from isolated ionic aggregates which had a core equivalent to an ionic cluster and a shell formed by ion pairs and multiplets. The steric hindrance between the polymer backbone chains was certainly the cause of the separation between the central core and the rest of the ion pairs. It was the interference between the core and the shell that contributed to the ionic peak. No interaggregate interference was present. Therefore, it is often referred to as an intraparticle interference model, or simply as the core–shell model.

Let the radius of the core (with an electron density difference d_1 between the ion cluster and the hydrocarbon backbone background) be R_1 and the inner and outer radii of the shell (with an electron density difference d_2) be respectively R_2 and R_3. The form factor of this core–shell particle, $P_{\text{Core-Shell}}(q)$, has the form

$$P_{\text{Core-Shell}}(q) = [v_1 d_1 \Phi(qR_1) + v_3 d_2 \Phi(qR_3) - v_2 d_2 \Phi(qR_2)]^2 \tag{17}$$

where

$$\Phi(x) = \left[\frac{3(\sin x - x\cos x)}{x^3}\right]^2 \quad \text{and} \quad v_k = (4\pi/3)R_k^3$$

In the absence of interparticle interference, the structure factor is equal to 1. Thus, the scattered intensity is a sum of the scattering from each core–shell particle. For N core–shell particles in scattering volume V, the scattered intensity becomes $NP_{\text{Core-Shell}}(q)$. Not counting N, the core–shell model is a five-parameter model in an analysis of the SAXS profile in relative units.

Equation 17 can predict a small scattering angle upturn from which a radius of gyration of the core–shell could be determined according to the Gunier law.

Figure 1 shows a few scattering profiles calculated using eq 17. We fixed R_1 = 1 nm and d_2 = 1 (arbitrary unit) while changing R_2, R_3, and d_1. All curves have been normalized to 1 at q = 0. The "ionic peak" becomes more and more pronounced with the decrease in the electron density difference between the core and the shell. The peak shifts to a lower q value when the spacing between

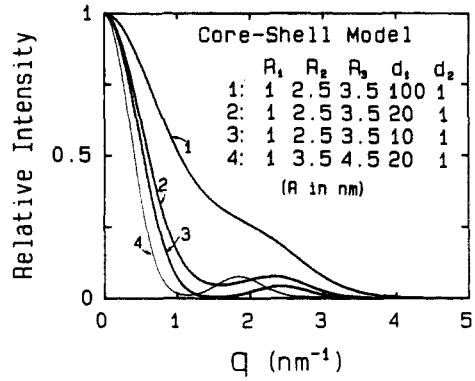

Figure 1. Selected scattering profiles computed based on the core–shell model. A peak is observed for curves 2–4, mimicking the SAXS ionic peak. The electron densities d_1 and d_2 are in relative units. All curves are normalized to 1 at q = 0.

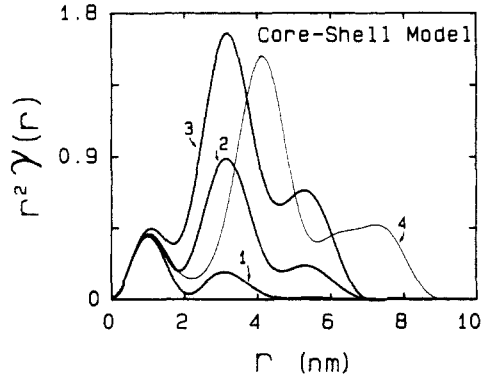

Figure 2. Correlation functions, $p(r) = r^2\gamma(r)$, corresponding to the scattering profiles in Figure 1. The first maximum from the origin is due to the interference from the core. The second maximum is due to the interference between the core and the shell. The third maximum is a consequence of the interference from the shell. The correlation functions are always of positive values and fall to zero magnitude at $r = 2R_3$.

the core and the shell is increased. It is also noted that the peak position corresponds to a Bragg spacing that is close to R_2 (for curves 2 and 4 where the ionic peak is well formed). We used I versus q, instead of log I versus q, in order to emphasize the ionic peak characteristics of the core–shell model.

The correlation functions of the scattering profile in Figure 1 can be obtained numerically according to eqs 11 and 16. Figure 2 shows their corresponding correlation function, $p(r) = r^2\gamma(r)$. $p(r)$ is often called the distance distribution function, since it measures the probability of finding two scattering points that are spaced by a distance of r. It is obvious that the correlation functions are always positive. As a general feature for all intraparticle interference models, the correlation functions reach zero magnitude at a maximum spacing in the core–shell particle, i.e., $2R_3$. Three maxima can be observed. The first maximum from the origin has a peak located at $r = R_1$ (from the interference of the core). The second maximum peaks at $(R_2 + R_3)/2$ (from the interference between the core and the shell). The third one is due to the interference of the shell.

It should be mentioned that a model assuming a lamellar-shaped core–shell was also proposed.[22] We shall consider the lamellar-shaped core–shell model as a variation of the *intraparticle* interference model and use the original core–shell model as a representative approach based on intraparticle interference only.

IV.2. Modified Core–Shell Model.[23] Fujimura et al.[23] proposed an alternative core–shell model to interpret the

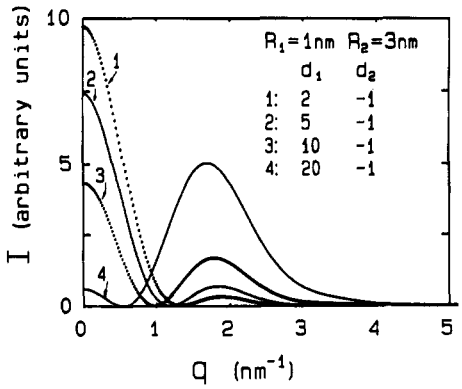

Figure 3. Selected scattering profiles computed based on the modified core–shell model. A peak at $q \sim 1.8$ nm^{-1} is observed for all curves with $R_1 = 1$ nm and $R_2 = 3$ nm, mimicking the SAXS ionic peak. The electron densities d_1 and d_2 are in relative units. Radii of gyration cannot be predicted as the electron density difference between the core and the shell is increased.

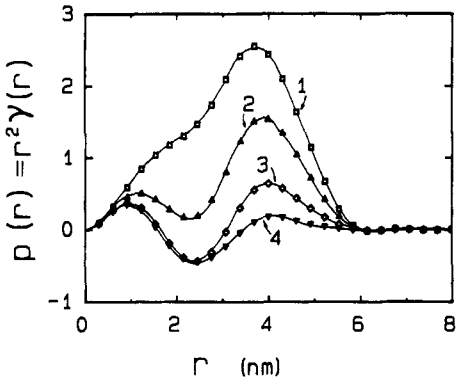

Figure 4. Correlation functions, $p(r) = r^2\gamma(r)$, corresponding to the scattering profiles in Figure 3. The first maximum from the origin is due to the interference from the core. The second maximum is due to the interference between the core and the shell. The correlation functions can have negative values and terminate at $r = 2R_2$.

SAXS results. The model also used a spherical core with a radius R_1 and an electron density d_1 to represent an ionic aggregate. The shell with an outer radius R_2 and an electron density d_2 was actually formed by the hydrocarbon chains whose steric character prevented more ion pairs from further aggregation. The model also assumed no interparticle interference, although it allowed an ionic atmosphere (formed by ions pairs) to be present outside of the core–shell whose electron density was lower than that of the core while higher than that of the shell. The model attributes the ionic peak to the interference between the ionic core and the hydrocarbon shell with a negative electron density.

The structure factor for this modified core–shell, $P_{\text{M-Core-Shell}}(q)$, is given by eq 18

$$P_{\text{M-Core-Shell}}(q) = [v_1(d_1 - d_2)\Phi(qR_1) + v_2 d_2 \Phi(qR_2)]^2 \quad (18)$$

with v and Φ being defined in eq 17. Figure 3 shows four sets of scattering profiles with fixed values of $R_1 = 1$ nm, $R_2 = 3$ nm, and $d_2 = -1$ (arbitrary units). When d_1 is changed from 2 to 20, the ionic peak is slightly shifted to a lower q.

The corresponding correlation functions are shown in Figure 4, with labels from 1 to 4 being the same as those in Figure 3. The correlation functions, except for curve 1, show two maxima, with the first (from the origin) representing the interference of the core itself and the second the interference from the shell. The correlation function can be negative because of a relatively negative electron density of the shell. The first maximum peaks at R_1, while the second one approaches $(R_1 + R_2)/2$. As an intraparticle interference model, the correlation functions terminate at $2R_2$.

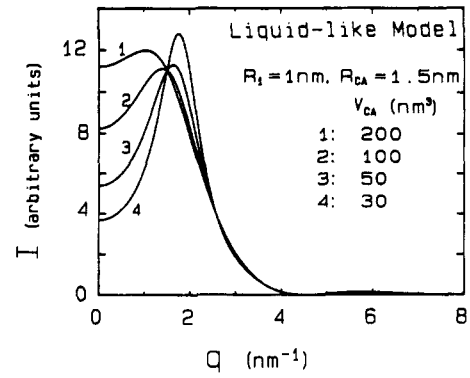

Figure 5. Selected scattering profiles computed based on the liquidlike model. With $R_1 = 1$ nm and $R_{CA} = 1.5$ nm, a decrease in v_p accompanies a sharpening in the SAXS ionic peak. The small-angle upturn cannot be predicted.

IV.3. Liquidlike Model.[24] Yarusso and Cooper assumed that ionic aggregates were of uniform spheres which had a liquidlike spatial arrangement. By introducing a new parameter, R_{CA}, the radius of closest approach between the spheres, to a liquid structure factor, i.e., by replacing the radius of the spheres, R_1, with R_{CA}, the authors were able to take a shell of hydrocarbon chains into account in the proposed model. The model assumed that the interparticle interference governed by a hard-sphere potential was the sole source responsible for the ionic diffraction peak.

The failure of predicting a small-angle upturn has been a shortcoming of the model.[25,26] The model, however, appears to fit the SAXS ionic peak better than core–shell models, though there are only three parameters in relative scale. The scattered intensity for the liquidlike model has the form

$$I(q) = N v_1^2 d^2 \Phi(qR_1)^2/[1 + (8v_{CA}/v_p)\Phi(2qR_{CA})] \quad (19)$$

where N is the number of spherical ionic aggregates in scattering volume V, $v_1 = (4\pi/3)R_1^3$, $v_{CA} = (4\pi/3)R_{CA}^3$, and v_p is the mean volume occupied by each sphere.

Figure 5 shows a set of four scattering profiles generated from eq 19. With $R_1 = 1$ nm and $R_{CA} = 1.5$ nm, a change in v_p from 200 to 30 nm^3 (increasing the relative volume fraction of the spheres) sharpens the ionic peak and moves the peak toward larger q values. As expected, no small-angle scattering (an upturn) is observed. The second peak at $q \sim 6$ nm^{-1} is the higher order peak from the form factor of a sphere.

Figure 6 plots the correlation functions which are numbered according to Figure 5. Similar to Figure 4, the first maximum from the origin is originated from the interference of the sphere (core). The liquid structure factor produces the rest of the maxima. The damping oscillations are the typical features of a liquid structure. The maxima other than the first one depend strongly on R_{CA} but rather weakly on v_p. The second maximum position measures the most probable intersphere spacing.

The determination of model parameters from correlation functions does not require a curve fitting. From the position of the first maximum, R_1 is determined. By matching the second peak position, R_{CA} is obtained. Then, the height of the second maximum yields v_p.

In comparison with Figure 4, it is noted that the appearance of the third maximum is very important in

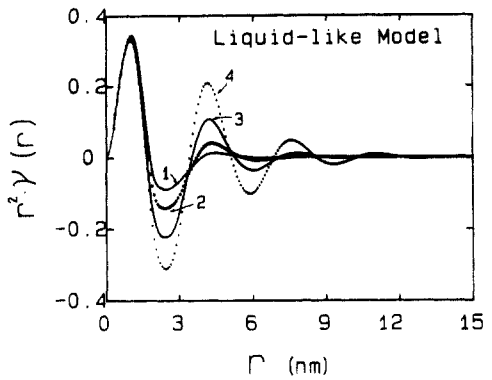

Figure 6. Correlation functions, $p(r) = r^2\gamma(r)$, corresponding to the scattering profiles in Figure 5. The first maximum from the origin is due to the interference from the core. The maxima other than the first one are due to the interparticle interference between the ionic aggregates. The correlation functions show damping oscillations. The peak position of those maxima depends strongly on R_{CA}, while the amplitude depends on v_p.

differentiating between an interparticle interference model, e.g., a liquidlike structure and an intraparticle interference model like a modified core–shell structure.

It is also noted that curve 4 in Figure 6 with $v_p/v_{CA} \sim 14$ hardly shows the third maximum. A v_p/v_{CA} value of about 10 is probably an experimental onset for a sufficient demonstration of the presence of liquidlike interparticle interference.

V. Results and Discussion

In the present study, we have measured the following SAXS profiles using the NSLS synchrotron X-ray source: (1) SPS-Na (4.5 mol % of sulfur, 100% neutralized, $M_w/M_n = 1.2$), $q_{min} = 0.035$ nm^{-1}, $q_{max} = 8$ nm^{-1}, and $I(q_{max})/I(q_{min}) < 2 \times 10^{-5}$; (2) SPS-Zn (4.5 mol % of sulfur, 100% neutralized, $M_w/M_n = 1.2$), $q_{min} = 0.035$ nm^{-1}, $q_{max} = 8$ nm^{-1}, and $I(q_{max})/I(q_{min}) < 2 \times 10^{-4}$ where $q = (4\pi/\lambda)\sin(\theta/2)$, and $\lambda = 0.154$ nm.

The experimental details, including polymer and sample preparation as well as SAXS settings and method of data correction, have been described elsewhere.[25,26] If a system has both a short-range structure and a completely random distribution of such a structure in the long range, i.e., the correlation length is much larger than the length scale of the local structure, the scattered intensity can be separated approximately into two parts:[25,26] $I(q) \cong I_{structure}(q) + I_{D-B}(q)$ in which we have relaxed the definition of $I_{structure}$ as based on the ionomer morphological models. Following eqs 8 and 11, the distance distribution function $r^2\gamma(r) = p(r)$ has the form

$$p(r) = p_{structure}(r) + r^2 \exp(-r/a) \qquad (20)$$

At *large* r, $p(r) \sim r^2 \exp(-r/a)$, which has a maximum at $r = 2a$.

Practically, if one determines the correlation length a from the maximum value of $p(r)$, one should be able to obtain the correlation function $p_{structure}(r)$ using eq 20.

Figure 7 shows the measured SAXS profile (dots) of a SPS sodium salt (4.5 mol % sulfur, 100% neutralization, $Mw = 1.15 \times 10^5$, and $M_w/M_n = 1.04$) after subtraction of the scattered intensity of the polystyrene (PS) backbone.[26] The curve was smoothed using respectively a three-point smoother repeating 100 times (thick line) and a cubic-spline smoother (thin line). We deliberately oversmooth the curve using a cubic-spline smoother in order to determine the sensitivity of data smoothing on the final correlation function. A linear plot of the measured and

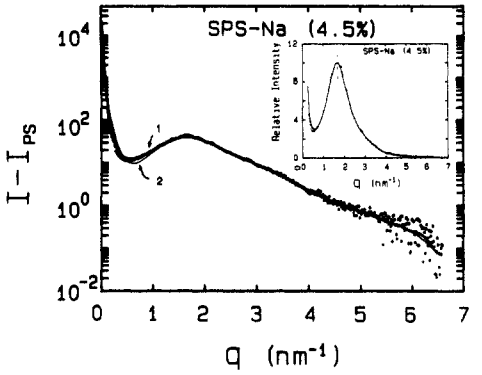

Figure 7. Plot of $I - I_{PS}$ versus q for SPS-Na[6] (4.5 mol %). Solid circles denote experimental data. The thick line (curve 1) denotes three-point smoothing, while the thin line (curve 2) denotes cubic-spline smoothing. The inset shows that, even with a three-point smoothing, the data were slightly oversmoothed.

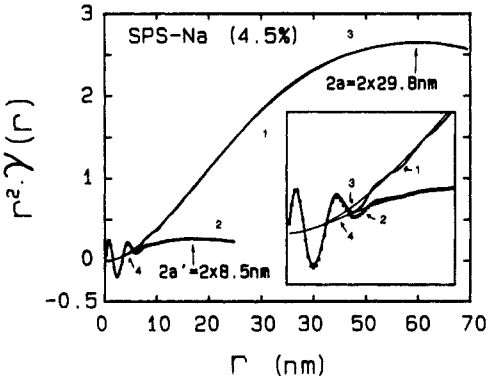

Figure 8. Plot of $r^2\gamma(r)$ (long-range inhomogeneities) versus r (nm) for SPS-Na (4.5 mol %). The Debye–Bueche model could fit the SAXS profile reasonably well over a range of q. Deviation from the Debye–Bueche model is expected.

smoothed (three-point smoother) SAXS curves is shown in the inset of Figure 7. Even the three-point smoothing represents slight oversmoothing because the ionic peak is less sharp and the small-angle upturn has become less sharp. It should be noted that the unsmoothed SAXS data were based on measurements by a very high resolution linear position-sensitive detector. High-frequency oscillations would occur unnecessarily in the correlation function without signal averaging. The results after smoothing show a more realistic physical picture. Oversmoothing is used to demonstrate that its effect does not alter our conclusions.

Figure 8 shows the correlation function for the SPS sodium salt (4.5 mol % of sulfur, 100% neutralization, and $M_w/M_n = 1.04$) obtained from the smoothed experimental SAXS curve using respectively a three-point smoother (curve 1) and a cubic-spline smoother (*dotted* curve 2). The long-range inhomogeneity is clearly demonstrated. Curve 1 has a maximum at $r_{max} = 2a$, with $a = 29.8$ nm. $p_{D-B}(r) = r^2e^{-r/a}$ was computed and plotted (curve 3). A nearly perfect match for curves 1 and 3 was obtained. Dotted curve 2 shows a maximum at 17 nm. A similar $p_{D-B}(r)$ (curve 4) also shows a good match between dotted curve 2 and curve 4. $p(r)$ at small r contains short-range structural information of the ionomer that is insensitive to the smoothing procedure.

Basically, the smoothed experimental curves were represented by curve 1 and dotted curve 2. They were not the same, because the SAXS data had been oversmoothed; slightly for curve 1 but more so for dotted curve 2 in the small q (or large r) range. However, in the short r-range, the experimental results become identical. Thus, in a

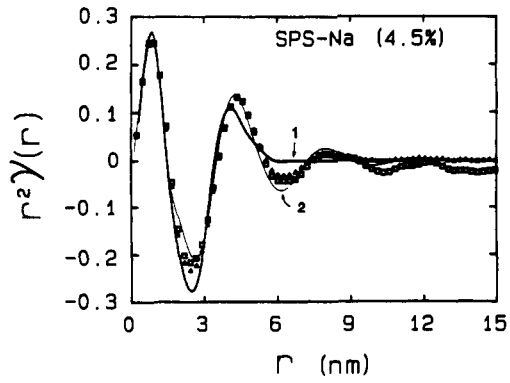

Figure 9. Plot of $r^2\gamma(r)$ (local structures) versus r (nm) for SPS-Na (4.5 mol %). Solid triangles denote experimental data using a cubic-spline smoother. Hollow squares denote experimental data using a three-point smoother. Curve 1 was computed from the modified core–shell model, and curve 2 was based on the liquidlike model.

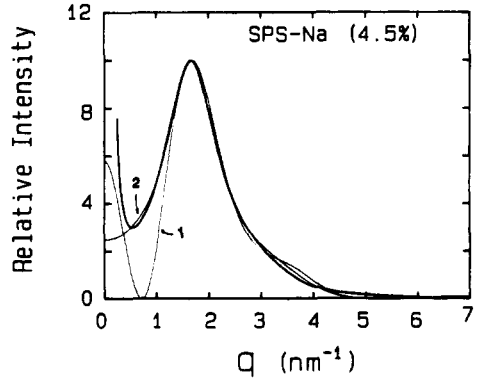

Figure 10. Comparison of experimental and computed $I(q)$, with curves 1 and 2 denoting the modified core–shell model and the liquidlike model, respectively. Both models can fit the ionic peak. However, the liquidlike model appears to follow the peak profile over a larger q range at $q < q_{peak}$. The small-angle upturn of the core–shell model cannot be used to fit the experimental small-angle upturn.

comparison of the experimental data with the morphological models, oversmoothing had little effect on our conclusions. Second, the Debye–Bueche model (curves 3 and 4) merely provided a base line for the experimental curve in the large q (or small r) range, as shown in the inset of Figure 8.

The net correlation function for the SPS sodium salt (4.5 mol % of sulfur, 100% neutralization, and M_w/M_n = 1.04) is shown in Figure 9. The hollow squares were obtained from Figure 8 by subtracting $p_{D-B}(r)$ from $p(r)$ (using a three-point smoother). The solid triangles were obtained similarly (using a cubic-spline smoother). The thick line (curve 1) was computed using the modified core–shell model with R_1 = 0.85 nm, R_2 = 3.2 nm, d_1 = 30, d_2 = −1, and v_p = 1 nm^3. The thin line (curve 2) was computed using the liquidlike model with R_1 = 0.85 nm, R_{CA} = 1.6 nm, and v_p = 40 nm^3. It appeared that both models could fit the experimental correlation function reasonably well up to $r \sim 4$ nm. However, only the liquidlike model could fit the curve for ~ 4 nm $< r < \sim 10$ nm with a *second* minimum. No significant difference in using the smoothing procedure was observed for $r < \sim 10$ nm.

Figure 10 shows the smoothed SAXS profile (thick line, using a three-point smoother) for a SPS sodium salt (4.5 mol % of sulfur, 100% neutralization, and M_w/M_n = 1.04). The computed SAXS profiles for the modified core–shell model (curve 1) and for the liquidlike model (curve 2) with the parameters shown in Figure 9 suggest that the

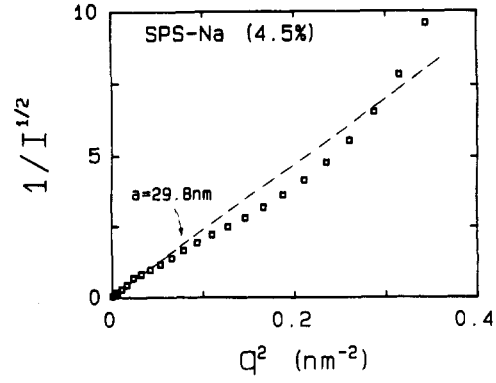

Figure 11. Plot of $I^{-1/2}$ versus q^2 based on a Debye–Bueche model. However, the scattered intensity (denoted by the hollow squares) was obtained by subtracting the computed scattering curve based on the liquidlike model from the smoothed SAXS curve in Figure 7.

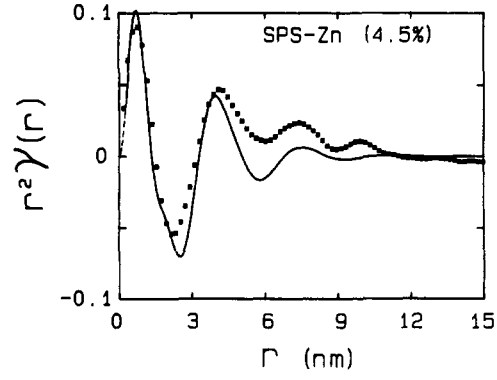

Figure 12. Plot of $r^2\gamma(r)$ (local structures) versus r for SPS-Zn (4.5 mol %). The solid line denotes the liquidlike model, while hollow squares denote experimental data[25] after three-point smoothing.

liquidlike model could fit the measured SAXS data better than the modified core–shell model at larger r or here at small q, except at $q < \sim 0.5$ nm^{-1} where the small-angle upturn is shown. The small-angle upturn could be fitted approximately by the Debye–Bueche inhomogeneity term as expressed by $I_{D-B}(q)$ in eq 9.

The difference between the smoothed SAXS curve and the computed curve from the liquidlike model in Figure 10 was plotted in Figure 11 in terms of $I^{-1/2}$ vs q^2. With eq 9 the correlation length can be determined by plotting $I_{D-B}^{-1/2}$ vs q^2. The dashed line represents such a plot with a = 29.8 nm. The deviation from the straight dashed line might be caused by uncertainty in the background subtraction. Nevertheless, the agreement is remarkable because here we have subtracted the short-range order instead of the procedures shown in Figure 8.

Figure 12 shows a plot of the correlation function (hollow squares) for SPS zinc salt (4.5 mol % of sulfur, 100% neutralization, and M_w/M_n = 1.04). A similar method used to get the correlation function for SPS-Na, as shown in Figure 9, was applied. $a \cong 9$ nm with a three-point smoother. The solid line in Figure 12 represents the liquidlike model fitted with R_1 = 0.72 nm, R_{CA} = 1.5 nm, and v_p = 40 nm^3. A systematic deviation from zero for $r > \sim 6$ nm could be attributed to an improper subtraction of the long-range order with the one-term Debye–Bueche model. Yet the liquidlike model could fit the experimental curve reasonably well. The fitting could also be improved by considering the polydispersity effect in the size of ionic aggregates.

We can fit the long-range inhomogeneity portion of the SAXS profile (at small scattering angles) more precisely

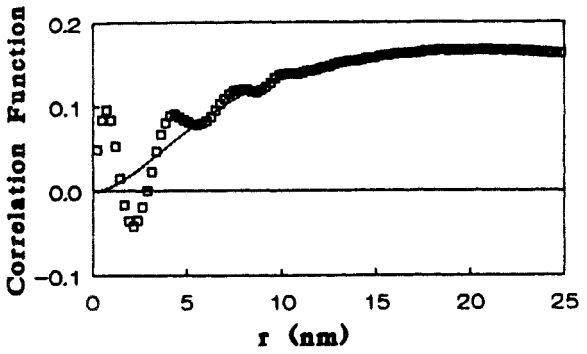

Figure 13. Correlation function, $p(r) = r^2\gamma(r)$, of SPS-Zn (4.5 mol %) (hollow squares) and fitting of a two-term Debye–Bueche type equation (solid line).

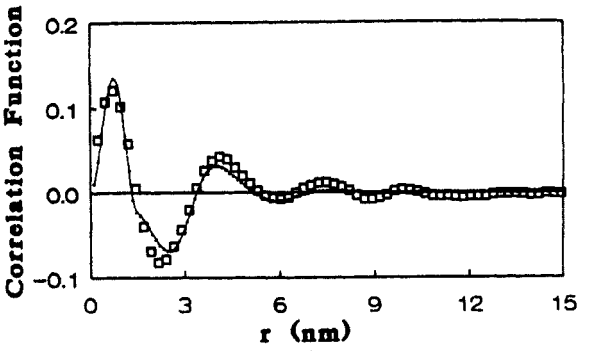

Figure 14. Difference correlation function (local structures), $p_{structure}(r)$ [$\equiv p(r) - r^2\gamma_{D-B}(r)$], of SPS-Zn (4.5 mol %) after a better match of the long-range inhomogeneities by using an additional fitting parameter in the Debye–Bueche equation. The local structure can be fitted well by a correlation function from the liquidlike morphological model (□) with $R_1 = 0.75$ nm, $R_{CA} = 1.5$ nm, and $v_p = 60$ nm^3.

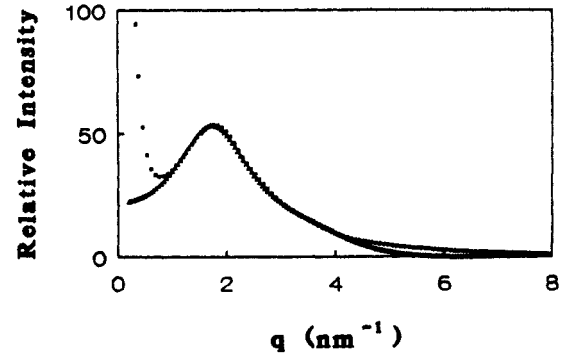

Figure 15. Comparison of SAXS difference profile ($I - I_{PS}$) and the scattering profile from the liquidlike model with the model parameters as shown in Figure 14. The ionic peaks are matched well for $1 < q < 4$ nm^{-1}.

by arbitrarily introducing an additional parameter. The physical reason could be that the inhomogeneities are not completely random. Figure 13 shows a correlation function which has been fitted with a two-term Debye–Bueche type equation. A more precise match of experimental and theoretical curves over a larger r-range could yield a difference correlation function which falls near zero at large r, as shown in Figure 14. In q-space, Figure 15 shows that the computed SAXS profile (triangles) from the liquidlike model using the parameters of Figure 14 matches well with the experimental SAXS difference profile (squares) over an appreciable q range ($1 < q < 4$ nm^{-1}).

VI. Conclusion

Correlation function analysis on the SAXS profiles for 4.5 mol % SPS sodium and zinc salts showed that the ionomer morphology could be well-represented by a short-range liquidlike structure in combination with an approximate long-range random inhomogeneity. The short-range structure determination was insensitive to the data smoothing procedures which we have employed.

A correlation length of random systems could be obtained better in r-space (correlation function) than in q-space, i.e., by empirically fitting the Debye–Bueche model directly to a SAXS profile if such systems possess a short-range structure. The correlation lengths are about 30 and 9 nm for SPS-Na and SPS-Zn, respectively. The length scale, however, is approximate since we do not expect the Debye–Bueche model to hold over a large q-range. It should also be noted that we do not consider the Debye–Bueche model to be an exact representation of the long-range inhomogeneities. Furthermore, even though ASAXS shows that the long-range inhomogeneities have the origin coming from Zn ions and are not due to voids, the nature of the long-range inhomogeneities remain unspecific. There could be some Zn salts or ion-cluster domains or inhomogeneities of the ionic background contributing toward the small scattering angle upturn in the scattered intensity. Also, the method of preparation (by compression molding) and the short annealing time have not established the fact that the ionomer films have reached an equilibrium structure.

Both the modified core–shell model and the liquidlike model could fit the experimental correlation function at small r values. The models could be used to determine the radius of the core of the ionic aggregates yielding 0.85 and 0.72 nm, respectively, for SPS-Na and SPS–Zn. The experimental correlation function showed a feature (second minimum in Figure 9) of interparticle interference that could not be explained by the intraparticle interference models.[20,23] While our SAXS data signify a better fit in the small r range using the liquidlike model, in the final analysis the lack of feature in the SAXS curve for ionomers clearly suggests that one may use a variety of morphological models to fit the SAXS experimental data and a definitive test for a specific model will most likely take more than the SAXS experiments above to confirm.

Acknowledgment. Support of this work by the National Science Foundation, Polymers Program (DMR-8921968), and of the SAXS facilities by the Department of Energy is gratefully acknowledged.

References and Notes

(1) Debye, P.; Bueche, A. M. *J. Appl. Phys.* **20**, 518.
(2) Brumberger, H.; Debye, P. *J. Phys. Chem.* **1957**, *61*, 1623.
(3) Chu, B.; Creti, D. M. T. *J. Phys. Chem.* **1967**, *71*, 1943.
(4) Koberstein, J. T.; Picot, C.; Benoit, H. *Polymer* **1985**, *26*, 673.
(5) Clough, S. B.; Cortelek, D.; Nagabhushanam, T.; Salamone, J. C.; Watterson, A. C. *Polym. Eng. Sci.* **1984**, *24*, 385.
(6) Wu, D. Q.; Phillips, J. C.; Lundberg, R. D.; MacKnight, W. J.; Chu, B. *Macromolecules* **1989**, *22*, 992.
(7) See for examples: Guinier, A.; Fournier, G. *Small Angle Scattering of X-Rays*; Wiley: New York, 1955. *Small Angle X-Ray Scattering*; Glatter, O., Kratky, O., Eds.; Academic Press: London, 1982.
(8) Cooley, J. W.; Tukey, J. W. *Math. Comput.* **1965**, *19*, 297.
(9) Lado, F. *J. Comput. Phys.* **1971**, *8*, 417.
(10) See for example: Chu, B.; Xu, R. *Rev. Sci. Instrum.* -1989, *60*, 910.
(11) See for example: Reinsch, C. H. *Numerische Mathematik* **1967**, *10* (3), 177.
(12) Anastasiadis, S. H.; Chen, J.-K.; Koberstein, J. T.; Siegel, A. F.; Sohn, J. E.; Emerson, J. A. *J. Colloid Interface Sci.* **1987**, *119*, 55.
(13) Shannon, C. *Bell. Sys. Tech. J.* **1948**, *27*, 379 and 623.

(14) Jaynes, E. T. In *Papers on Probability, Statistics and Statistical Physics*; Rosenkrantz, R., Ed.; Reidel: Dordrect, Holland, 1983.
(15) Skilling, J.; Bryan, R. K. *Mon. Not. R. Astron. Soc.* **1984**, *211*, 111.
(16) MacKnight, W. J.; Earnest, T. R. *J. Polym. Sci: Macromol. Rev.* **1981**, *16*, 41.
(17) Mauritz, K. A. In *Structure and Properties of Ionomers*; Pineri, M., Eisenberg, A., Eds.; Reidel: Dordrecht, Holland, 1986.
(18) Eisenberg, A. *Macromolecules* **1970**, *3*, 147.
(19) Eisenberg, A.; Hird, B.; Moore, R. B. *Macromolecules* **1990**, *23*, 4098.
(20) MacKnight, W. J.; Taggart, W. P.; Stein, R. S. *J. Polym. Sci., Polym. Symp.* **1974**, *45*, 113.
(21) Kao, J.; Stein, R. S.; MacKnight, W. J.; Taggart, W. P.; Cargill, G. S. *Macromolecules* **1974**, *7*, 95.
(22) Earnest, T. R., Jr.; MacKnight, W. J. *Macromolecules* **1977**, *10*, 206; *J. Polym. Sci., Polym. Phys. Ed.* **1978**, *16*, 143.
(23) Fujimura, M.; Hashimoto, T.; Kawai, H. *Macromolecules* **1981**, *14*, 1309; **1982**, *15*, 136.
(24) Yarusso, D. J.; Cooper, S. L. *Macromolecules* **1983**, *16*, 1871; *Polymer* **1985**, *26*, 371.
(25) Ding, Y. S.; Hubbard, S. R.; Hodgson, K. O.; Register, R. A.; Cooper, S. L. *Macromolecules* **1988**, *21*, 1698.
(26) Chu, B.; Wu, D. Q.; MacKnight, W. J.; Wu. C.; Phillips, J. C.; LeGrand, A.; Lantman, C. W.; Lundberg, R. D. *Macromolecules* **1988**, *21*, 523.